ACS central science

http://pubs.acs.org/journal/acscii

Research Article

Breaking Scaling Relationships in CO_2 Reduction on Copper Alloys with Organic Additives

Yungchieh Lai,[†] Nicholas B. Watkins,[†] Alonso Rosas-Hernández, Arnaud Thevenon, Gavin P. Heim, Lan Zhou, Yueshen Wu, Jonas C. Peters,* John M. Gregoire,* and Theodor Agapie*

Cite This: https://doi.org/10.1021/acscentsci.1c00860

Read Online

ACCESS | Metrics & More | Article Recommendations | Supporting Information

ABSTRACT: Boundary conditions for catalyst performance in the conversion of common precursors such as N_2, O_2, H_2O, and CO_2 are governed by linear free energy and scaling relationships. Knowledge of these limits offers an impetus for designing strategies to alter reaction mechanisms to improve performance. Typically, experimental demonstrations of linear trends and deviations from them are composed of a small number of data points constrained by inherent experimental limitations. Herein, high-throughput experimentation on 14 bulk copper bimetallic alloys allowed for data-driven identification of a scaling relationship between the partial current densities of methane and C_{2+} products. This strict dependence represents an intrinsic limit to the Faradaic efficiency for C−C coupling. We have furthermore demonstrated that coating the electrodes with a molecular film breaks the scaling relationship to promote C_{2+} product formation.

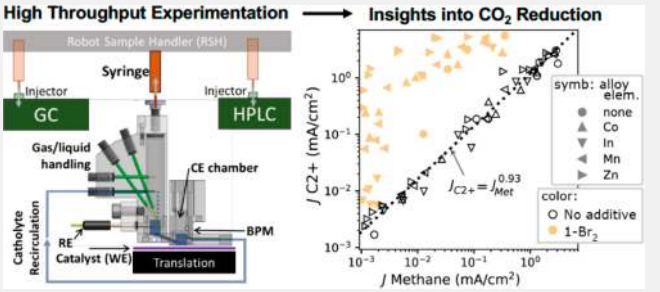

INTRODUCTION

The development of high-performing catalysts for sustainable and economically viable transformations remains a central goal of the chemical industry.[1] Chemical transformations are controlled by thermodynamic and kinetic rate laws that manifest as linear scaling relationships. Such relationships relating structure, activity, and reaction conditions are established for a range of reactions, including H_2O oxidation and N_2, O_2, CO_2, and H_2O reduction performed on both heterogeneous and homogeneous catalysts.[1−7] Because they provide theoretical or empirical trends for a particular chemical process, these scaling relationships not only help explain chemical reactivity but also guide the rational design of new and improved catalysts. Determining the underlying connections in chemical processes is particularly desirable toward deconvoluting fundamental selectivity limitations and targeting specific products.[2,8] Typically, the experimental establishment and breaking of scaling relationships, including mapping of volcano plots, deals with a small set of data points, a limitation that is sometimes compensated for by expansion of data sets through computation. Our development of high-throughput electrochemistry coupled to an automated product distribution analysis provides new opportunities for identifying scaling relationships.[9,10] Herein, we demonstrate a combination of catalyst design, high-throughput experimentation, and data science as a paradigm shift in both the identification of scaling relationships and the discovery of strategies for breaking them. We focus on applying this approach to CO_2 reduction (CO_2R) on Cu-based electrodes, an area where mechanistic complexity has obscured the identification of scaling relationships, has hindered catalyst optimization, and warrants further investigation.[11]

As strategies to transform CO_2 at scale are considered for a more sustainable carbon economy, exploiting the unique ability of Cu to reduce CO_2 to C_{2+} hydrocarbons and oxygenates makes it an attractive catalyst for optimization. The complex pathways toward myriad reduced products of CO_2R on Cu stymie efforts for producing carbon-coupled products with high selectivity and have prompted investigation into the mechanism of the transformation.[11] Systematic trends affecting selectivity have been shown with respect to adsorption energy scaling relationships and pH variation at the electrode surface.[7,12−15] Promising strategies for improving CO_2R selectivity for C_{2+} products include changing catalyst morphology[16−19] and electrolyte composition,[14,20] employing bimetallic systems and alloys,[21−23] and adding organic modifiers.[24−29] While these techniques may facilitate altered product distributions, they are not amenable to identifying empirical scaling relationships due to substantial variation in catalyst preparation and electrochemical testing conditions across independent studies. It is consequently pertinent to

Received: July 16, 2021

conduct studies that systematically and broadly vary select parameters. We have identified bulk alloying of Cu as an underdeveloped, though promising, strategy for catalyst optimization, with a large parameter space available based on the metal identity and composition,[30,31] well suited for investigation using our high-throughput screening system.[9,10] Additionally, organic additives represent an attractive orthogonal parameter of catalyst design. They can impact performance in a manner that has seldom been achieved by tailoring inorganic electrocatalyst composition or morphology alone.[32]

Inspired by recent success using molecular films to enhance the selectivity of catalysts for CO_2R,[29,33−35] herein, we describe the generation of a uniquely broad and systematic CO_2R catalyst database by combining a Cu bimetallic alloying strategy with the use of organic additives. Selectivity analysis highlights the impact of integrating high-throughput experimentation and data science to discover a power-law scaling relationship between partial current densities of CH_4 and C_{2+} that is broken upon coating with an organic additive, demonstrating a fundamental limitation of CO_2R on Cu and a strategy to overcome it through hybrid inorganic−organic interfaces.

RESULTS AND DISCUSSION

To elucidate correlations in CO_2R, experiments were designed to observe a large dynamic range of catalyst properties while mitigating conflation with experiment parameters such as electrolyte composition and mass transport conditions. For the present work, we varied catalyst composition, applied potential, and molecular additive presence. The choice of Cu alloys was guided by our previous discovery that the alloying elements In, Co, Mn, and Zn alter the activity and selectivity of Cu in different ways, although that study was limited to the detection of H_2, CH_4, and C_2H_4.[10] Studying Cu alloys with each of these elements and with different concentrations that span face-centered cubic (fcc) alloys and intermetallic phases (XRD of homogeneous alloys shown in Figures S12−S16), we sought to obtain a more comprehensive map of the reactivity of Cu-based alloy catalysts and to identify any systematic trends. The molecular additive, *N*,*N*′-ethylene-phenanthrolinium dibromide (**1-Br$_2$**), was selected based on its ability to enhance Faradaic efficiency (FE) and geometric partial current densities for C_{2+} products upon forming a well-defined film on polycrystalline Cu, primarily composed of a *para-para* isomer of the one-electron reduced and dimerized phenanthrolinium (Figure 1a).[33]

The catalyst performance with or without the additive was evaluated by chronoamperometry (CA) at a series of up to 6 potentials with subsequent product analysis using the batch reactor flow system illustrated in Figure 1. This system uses rapid electrolyte flow, as opposed to vigorous CO_2 bubbling, to generate suitable and reproducible mass transport conditions. The rapid concentration of reaction products enhances measurement throughput by enabling shorter electrolysis and faster chromatography compared to traditional methods. Hybrid metal−organic electrodes were prepared via electrodeposition of organic films on the polycrystalline metal electrode from an aqueous 0.1 M $KHCO_3$ buffered electrolyte containing 0.1 mM **1-Br$_2$**. In total, experiments with 14 alloy catalysts and pure Cu provide electrochemical and partial current densities for 137 unique combinations of catalyst composition, additive presence, and applied potential, as

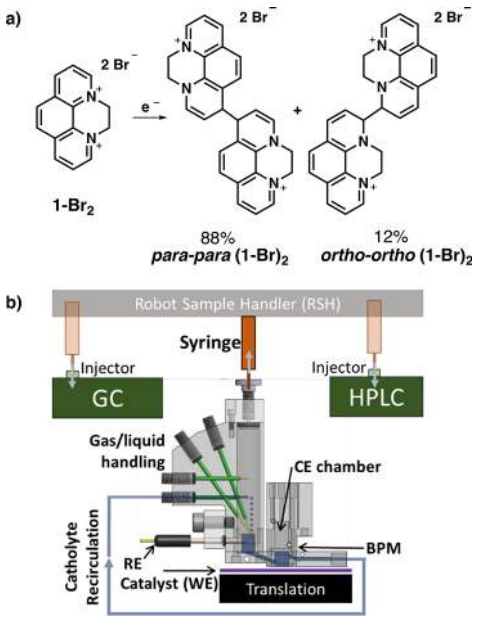

Figure 1. (a) The electrochemical reductive coupling of two **1-Br$_2$** molecules results in a mixture of two products; (b) The high throughput catalyst screening system where a select catalyst is positioned under a recirculating electrochemical batch reactor. After electrocatalyst operation, a robot sample handler (RSH) uses a syringe (orange) to extract aliquots from the headspace and then catholyte, with each aliquot injected into the respective analytical instrument (green, syringe positions in translucent orange) for gas or high-pressure liquid chromatography (GC, HPLC). The reference electrode (RE) is placed in the electrolyte inlet to the working electrode (WE) chamber, which is separated from the counter electrode (CE) chamber by a bipolar membrane (BPM).

shown for select Mn-doped catalysts in Figure 2a,b and for all catalysts in Figures S1 and S2.

Pairwise relationships of the geometric partial current density and the FE for representative products (Figure S5) highlight the effect of the combined strategy of alloying and organic films. The intrinsic modification of catalyst selectivity can be detected through analysis of the Pearson correlation coefficient of the logarithm of partial current densities. A close-to-unity positive correlation indicates that selectivity between the two products cannot be tuned with the parameters under consideration, which is indicative of a free-energy scaling relationship. A substantially negative correlation indicates a trade-off in selectivity, wherein enhanced formation of one product occurs at the expense of the other, which is indicative of kinetic competition for a shared reaction intermediate.

The large data set provided here via high-throughput experimentation enables the study of correlation coefficients and their modification (Figure 2). Previous work on polycrystalline Cu indicates that the kinetic regimes that govern the CO_2R product distribution differ with applied potential due to modulation of the energy landscape as a function of overpotential as well as second-order effects such as CO_2 mass transport and changes to the pH at the catalyst surface.[36,37] To facilitate the observation of how the catalyst itself affects selectivity, we aim to mitigate the influences from the extrinsic effects by limiting the overpotential range (−0.84 to −1.1 V vs reversible hydrogen electrode, RHE) and using rapid electrolyte flow over flat catalyst films with a maximum current density of 15 mA cm^{-2}, which promotes uniform mass

https://doi.org/10.1021/acscentsci.1c00860
ACS Cent. Sci. XXXX, XXX, XXX−XXX

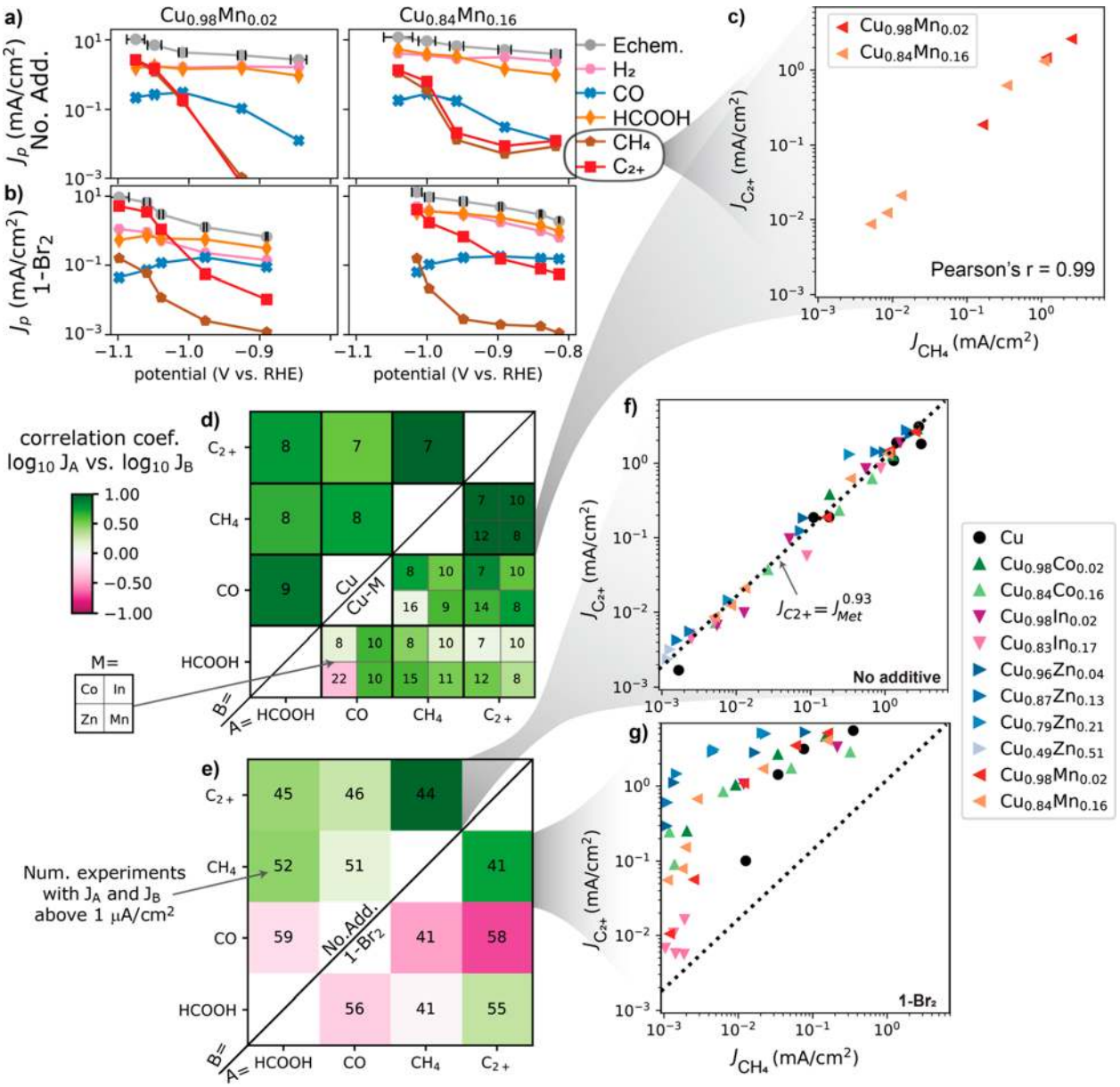

Figure 2. Illustration of acquired data and correlation analysis. The electrochemical and geometric partial current densities are shown for 5 electrolysis experiments with $Cu_{0.98}Mn_{0.02}$ and 6 electrolysis experiments with $Cu_{0.84}Mn_{0.16}$ catalysts, both (a) without additive and (b) with **1-Br$_2$**. Select products or product categories were considered for correlation analysis. For A = CH_4 and B = C_{2+}, part a contains 8 electrolysis experiments with geometric partial current densities for both A and B above 1 μA cm^{-2}. The corresponding 8 points are shown in part c and used to calculate the Pearson correlation coefficient to represent additive-free Cu−Mn alloys. This analysis was applied to all 6 pairwise combinations of the products HCOOH, CO, CH_4, and C_{2+} and repeated for pure Cu and each Cu−M alloy system. The resulting set of correlation coefficients is shown in part d. The printed numbers in each cell indicate the number of electrolysis experiments used in the calculation, for example, 8 for the A = C_{2+}, B = CH_4, and M = Mn cell corresponding to the plot in part c. This analysis was also applied to electrolysis experiments from all compositions, first with and then without **1-Br$_2$** additive, to assess the impact of the additive on the 6 pairwise correlation coefficients, as shown in part e. For A = C_{2+} and B = CH_4 in part e, the data underlying the correlation analysis are shown (f) without additive and (g) with **1-Br$_2$**, where points are colored according to their composition. The data in part f follow the power-law relationship indicated by the dashed line, which is also depicted in part g to show the extent by which the data with **1-Br$_2$** deviate from this power-law relationship. The horizontal error bars in part a estimate the variation in potential in each electrolysis, and the quantified uncertainty for each partial current density is smaller than the point size (see the Experimental Uncertainty section in the SI).

transport and limits pH gradients in the electrochemical reactor. This potential range includes the onset of substantial partial current density for highly reduced products, making alteration of correlation coefficients in this range a prime target for controlling product selectivity with catalyst modification. We first demonstrate a Pearson correlation analysis to ascertain the extent by which high correlation coefficients can be lowered via variation in catalyst composition. For example, the box in Figure 2d with A = CH_4 and B = C_{2+} shows a high correlation coefficient of 0.99 for these products when considering a series of 7 electrolysis experiments with a polycrystalline Cu catalyst in which partial current densities for both CH_4 and C_{2+} products varied from approximately 1 μA cm^{-2} to 3 mA cm^{-2}. The analogous analysis for polycrystalline

https://doi.org/10.1021/acscentsci.1c00860
ACS Cent. Sci. XXXX, XXX, XXX−XXX

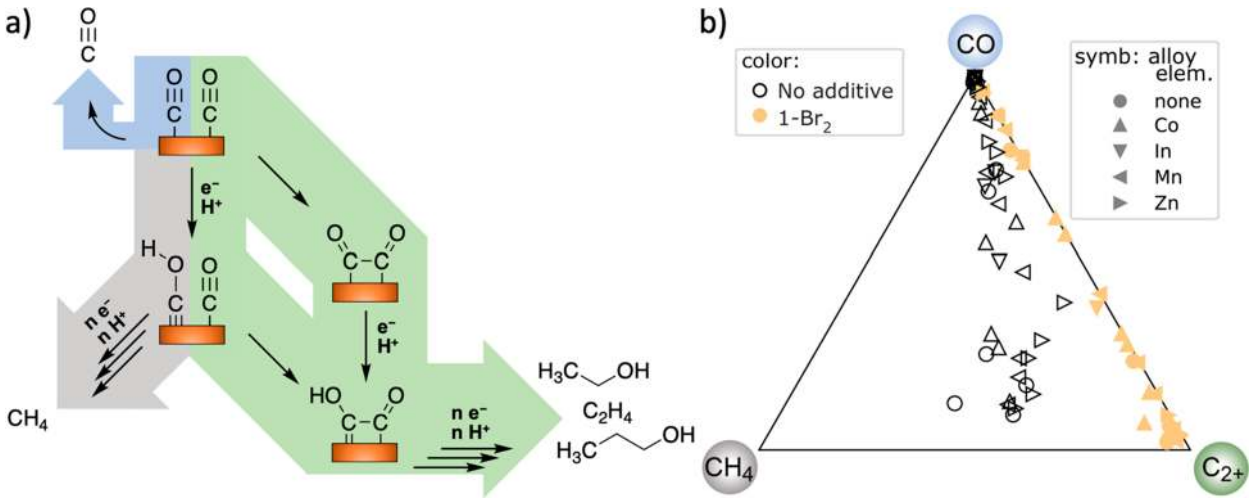

Figure 3. (a) Possible reaction mechanisms (selected from a multitude of variations previously proposed),[11] where pathways are highlighted in color with respect to their products in part b. There are two branching points between CH_4 and C_{2+} products that could be responsible for the relationship observed in Figure 2. The strong relationship between the gray and green pathways is broken with the addition of molecular additives, implying a potential change in mechanism. (b) Summary of molar selectivity for reduction of the CO* intermediate. Measured partial current densities for CO, CH_4, and C_{2+} products are converted to molar flux of CO* required to produce the respective products, whose normalization provides the ternary composition for inclusion in this figure. Each electrolysis experiment produces 1 data point that indicates the catalyst's selectivity with respect to the three reaction pathways highlighted in part a that start from the common CO* intermediate.

Cu−M alloys is summarized by the boxes with A = C_{2+} and B = CH_4, where the correlation coefficient was calculated for each alloying element using various combinations of alloy composition and applied potential. The source data and their utilization of a correlation analysis are illustrated for the Cu−Mn system in Figure 2a,c.

The total number of electrolysis conditions and range of alloy compositions (x in $Cu_{1-x}M_x$) are as follows: 7 conditions with M = Co and x = 0.02 or 0.16; 10 conditions with M = In and x = 0.02 or 0.17; 16 conditions with M = Zn and x = 0.04, 0.13, 0.21, or 0.51; and 8 conditions with M = Mn and x = 0.02 or 0.16. Despite the variation in composition and potential within each of these Cu−M systems, each correlation coefficient remains in excess of 0.98, and in total, the correlation coefficient for all Cu−M alloys is not meaningfully changed from that observed with pure Cu. Figure 2f shows the aggregation of data for Cu and its alloys, demonstrating that a power-law relationship is closely followed over a broad range of composition and applied potential. This striking relationship, over 3 orders of magnitude, in partial current densities strongly suggests that on these bulk alloy catalysts there is a common branching point, or combination of branching points, that consistently partitions between CH_4 and C_{2+} products (Figure 3a). Preservation of the CH_4/C_{2+} ratio as observed here represents a newly discovered fundamental limitation for efforts to improve selectivity through bulk bimetallic alloying alone.

A simple rationale for the near 1:1 ratio observed for CH_4 and C_{2+} products is challenged by the complexity of the mechanism of CO_2R.[38] Under different reaction conditions, such as using an alternate bicarbonate concentration, a similar power-law trend is observed, but with a slightly different slope (Figure S4). The up-shifted CH_4 to C_{2+} ratio agrees with the influence of $KHCO_3$ concentration where 0.1 M was considered to be the optimal environment for C_{2+} products.[13,14,39,40] The preservation of the scaling relationship is therefore supportive of an intrinsic mechanistic limitation for the production of methane and C_{2+} products for the set of experimental conditions used herein. Also, the alloying elements substantially alter other aspects of the product distribution, making this collection of catalyst electrodes particularly well-suited for inferring intrinsic reactivity trends; the catalyst morphology is kept relatively constant with respect to the compendium of results in the literature.[11,14,16,17,20−22,24−26,30,41] For example, through study of well-defined Cu surfaces, Hori and others identified that the relative production of CH_4 and C_2H_4 is highly facet-dependent.[15] The distribution of exposed facets of a polycrystalline fcc-phase metal electrode could be altered via alloying due to changes in growth kinetics and/or relative surface energies upon addition of the alloying element, which would in principle provide a method to break the CH_4/C_{2+} scaling relationship by tuning catalyst composition. However, the observation that the scaling relationship holds over a broad range of alloy compositions with distinct product distributions indicates that facet selectivity is not the main contributor in the observed product selectivity.

CO_2R to highly reduced products such as CH_4 and C_{2+} products proceeds via a common *CO intermediate.[42,43] Methane synthesis is proposed to proceed via a Langmuir−Hinshelwood pathway, where a surface *H couples with *CO to form a *CHO or *COH intermediate that is further hydrogenated toward methane.[42,44,45] Meanwhile, the production of C_{2+} products occurs via the coupling of two precursor *CO molecules, potentially involving intermediate *CHO or *COH adsorbates.[42,43] The absence of CO−CH_4 or CO−C_{2+} power-law relationships without the additive and the observation of a negative correlation coefficient between CO−-ethylene in the presence of the additive are consistent with kinetic competition for a common intermediate (Figure S5). Despite variation in free CO produced (Figure S19), for the conditions tested, the assumed variation of CO concentration near the surface of the electrode is inconsequential with respect to the CH_4−C_{2+} relationship. Therefore, although the specific mechanism or mechanisms remain debated and may involve multiple pathways depending on the

https://doi.org/10.1021/acscentsci.1c00860
ACS Cent. Sci. XXXX, XXX, XXX−XXX

morphology or crystal facet, the observed scaling relationship between CH_4 and C_{2+} indicates that the relative kinetics at the branching point(s), remarkably, remain rigorously locked at the same ratio over the many catalysts and applied potentials tested herein. Breaking this dependence is highly desirable for improved selectivity for C_{2+} products.

The Pearson correlation analysis was extended to the impact of the **1-Br$_2$** additive (Figure 2e), where the correlation coefficient for each set of conditions includes the aggregation of all catalyst compositions and potentials. Coating the catalysts using **1-Br$_2$** lowers the correlation coefficient for CH_4 and C_{2+} from 0.99 to 0.74, a striking alteration whose implication is that, within the range of catalyst compositions considered in the present work, tuning the selectivity between CH_4 and C_{2+} is only achieved in the presence of the additive, underscoring the importance of multimodal catalyst development.[46]

The basis by which the additive disrupts the scaling relationship between CH_4/C_{2+} (Figure 2f) by increasing C_{2+} production and suppressing CH_4 formation (Figure 2g) is of particular interest. Figure 3a illustrates the portion of the CO_2R reaction network wherein branching ratios dictate whether the common CO* intermediate results in the generation of CO, CH_4, or C_{2+} products. Figure 3b highlights how catalyst modification with the organic additive moves product distribution almost completely away from CH_4, to the $CO-C_{2+}$ vector of the graph. While accessing the CO-rich portion of the graph is commonplace in CO_2R electrocatalysis, the C_{2+}-rich portion of the graph is only accessed in the presence of **1-Br$_2$**.[11] The maximal selectivity was obtained with a $Cu_{0.85}Zn_{0.15}$ catalyst where 96% of the CO* intermediate was reduced to carbon-coupled products.

The breaking of the scaling relationship in the presence of **1-Br$_2$** cannot be explained by morphological changes or alloy segregation, as no nanostructuring was observed (Figures S7–S10, XRD in Figures S12–S16), therefore suggesting that the molecular additive improves selectivity via changes in the microkinetic pathway(s) in this system. The organic additive may affect CH_4-C_{2+} branching point(s) by (i) alleviating a rate limitation of the formation of the bound *CHO/*COH intermediate and lowering the barrier toward C–C coupling or (ii) promoting dimerization of the bound *CO relative to hydrogenation toward CH_4. In either case, kinetic competition for the *CO would be enhanced in the presence of the additive, which is consistent with the observation of a large and negative Pearson correlation between C_{2+} and CO (Figure 2e). We additionally note that neither of these explanations for the mechanism underlying the scaling law disruption has implications for the selectivity within the set of C_{2+} products. As shown in Figure S6, additional correlations among these products are observed both in the absence and in the presence of the molecular additive, motivating future tuning of the catalyst system to tackle other branching points in the reaction network for enhanced control over product selectivity.

CONCLUSION

High-throughput screening of the CO_2R activity and selectivity of Cu alloys with Co, In, Mn, and Zn revealed the propensity of organic additive **1-Br$_2$** to enable the development of hybrid electrocatalysts that can reduce CO_2 to high-order products with improved activity and selectivity. The large data set led to the observation of a CH_4-C_{2+} scaling relationship that demonstrates a particularly robust link between these products over a large range of conditions. The CH_4-C_{2+} relationship represents an intrinsic limitation of selectivity tuning through alloying. However, it can be disrupted to favor C_{2+} products by the presence of the organic additive, highlighting the potential of hybrid organic–inorganic catalysts to tune branching ratios in the CO_2R reaction network. These observations highlight the importance of data-driven identification of relationships that provide mechanistic insights to guide the study of complex reactions and catalyst development. Disentangling the possible explanations of the combined mechanistic influence of the additive and alloying elements will require substantial further investigation that will be guided by the observed data relationships elucidated in this study.

ASSOCIATED CONTENT

Supporting Information

The Supporting Information is available free of charge at https://pubs.acs.org/doi/10.1021/acscentsci.1c00860.

All material preparation and characterization, synthetic and electrochemical procedures, and raw data (PDF)

AUTHOR INFORMATION

Corresponding Authors

Jonas C. Peters − *Division of Chemistry and Chemical Engineering, California Institute of Technology, Pasadena, California 91125, United States*; Email: jpeters@caltech.edu

John M. Gregoire − *Division of Engineering and Applied Science, Liquid Sunlight Alliance, California Institute of Technology, Pasadena, California 91125, United States*; orcid.org/0000-0002-2863-5265; Email: gregoire@caltech.edu

Theodor Agapie − *Division of Chemistry and Chemical Engineering, California Institute of Technology, Pasadena, California 91125, United States*; orcid.org/0000-0002-9692-7614; Email: agapie@caltech.edu

Authors

Yungchieh Lai − *Division of Engineering and Applied Science, Liquid Sunlight Alliance, California Institute of Technology, Pasadena, California 91125, United States*

Nicholas B. Watkins − *Division of Chemistry and Chemical Engineering, California Institute of Technology, Pasadena, California 91125, United States*

Alonso Rosas-Hernández − *Division of Chemistry and Chemical Engineering, California Institute of Technology, Pasadena, California 91125, United States*

Arnaud Thevenon − *Division of Chemistry and Chemical Engineering, California Institute of Technology, Pasadena, California 91125, United States*

Gavin P. Heim − *Division of Chemistry and Chemical Engineering, California Institute of Technology, Pasadena, California 91125, United States*

Lan Zhou − *Division of Engineering and Applied Science, Liquid Sunlight Alliance, California Institute of Technology, Pasadena, California 91125, United States*

Yueshen Wu − *Division of Chemistry and Chemical Engineering, California Institute of Technology, Pasadena, California 91125, United States*; orcid.org/0000-0002-3784-0594

Complete contact information is available at: https://pubs.acs.org/10.1021/acscentsci.1c00860

https://doi.org/10.1021/acscentsci.1c00860
ACS Cent. Sci. XXXX, XXX, XXX−XXX

Author Contributions

†Y.L. and N.B.W. contributed equally to this work.

Notes

The authors declare no competing financial interest.

■ ACKNOWLEDGMENTS

This material is based on work performed by the Liquid Sunlight Alliance, which is supported by the U.S. Department of Energy, Office of Science, Office of Basic Energy Sciences, Fuels from Sunlight Hub under Award DE-SC0021266. A.T. acknowledges Marie Skłodowska-Curie Fellowship H2020-MSCA-IF-2017 (793471). The Resnick Sustainability Institute at Caltech is acknowledged for support of the laboratory facilities in which this research was conducted.

■ REFERENCES

(1) Seh, Z. W.; Kibsgaard, J.; Dickens, C. F.; Chorkendorff, I.; Nørskov, J. K.; Jaramillo, T. F. Combining Theory and Experiment in Electrocatalysis: Insights into Materials Design. *Science* **2017**, *355* (6321), No. eaad4998.

(2) Pérez-Ramírez, J.; López, N. Strategies to Break Linear Scaling Relationships. *Nat. Catal.* **2019**, *2* (11), 971−976.

(3) Greeley, J. Theoretical Heterogeneous Catalysis: Scaling Relationships and Computational Catalyst Design. *Annu. Rev. Chem. Biomol. Eng.* **2016**, *7* (1), 605−635.

(4) Liu, X.; Xiao, J.; Peng, H.; Hong, X.; Chan, K.; Nørskov, J. K. Understanding Trends in Electrochemical Carbon Dioxide Reduction Rates. *Nat. Commun.* **2017**, *8* (1), 15438.

(5) Waldie, K. M.; Ostericher, A. L.; Reineke, M. H.; Sasayama, A. F.; Kubiak, C. P. Hydricity of Transition-Metal Hydrides: Thermodynamic Considerations for CO $_2$ Reduction. *ACS Catal.* **2018**, *8* (2), 1313−1324.

(6) Ostericher, A. L.; Waldie, K. M.; Kubiak, C. P. Utilization of Thermodynamic Scaling Relationships in Hydricity To Develop Nickel Hydrogen Evolution Reaction Electrocatalysts with Weak Acids and Low Overpotentials. *ACS Catal.* **2018**, *8* (10), 9596−9603.

(7) Martin, D. J.; Wise, C. F.; Pegis, M. L.; Mayer, J. M. Developing Scaling Relationships for Molecular Electrocatalysis through Studies of Fe-Porphyrin-Catalyzed O2 Reduction. *Acc. Chem. Res.* **2020**, *53* (5), 1056−1065.

(8) Vojvodic, A.; Nørskov, J. K. New Design Paradigm for Heterogeneous Catalysts. *Natl. Sci. Rev.* **2015**, *2* (2), 140−143.

(9) Jones, R. J. R.; Wang, Y.; Lai, Y.; Shinde, A.; Gregoire, J. M. Reactor Design and Integration with Product Detection to Accelerate Screening of Electrocatalysts for Carbon Dioxide Reduction. *Rev. Sci. Instrum.* **2018**, *89* (12), 124102.

(10) Lai, Y.; Jones, R. J. R.; Wang, Y.; Zhou, L.; Richter, M. H.; Gregoire, J. The Sensitivity of Cu for Electrochemical Carbon Dioxide Reduction to Hydrocarbons as Revealed by High Throughput Experiments. *J. Mater. Chem. A* **2019**, *7* (47), 26785−26790.

(11) Nitopi, S.; Bertheussen, E.; Scott, S. B.; Liu, X.; Engstfeld, A. K.; Horch, S.; Seger, B.; Stephens, I. E. L.; Chan, K.; Hahn, C.; Nørskov, J. K.; Jaramillo, T. F.; Chorkendorff, I. Progress and Perspectives of Electrochemical CO_2 Reduction on Copper in Aqueous Electrolyte. *Chem. Rev.* **2019**, *119* (12), 7610−7672.

(12) Peterson, A. A.; Nørskov, J. K. Activity Descriptors for CO $_2$ Electroreduction to Methane on Transition-Metal Catalysts. *J. Phys. Chem. Lett.* **2012**, *3* (2), 251−258.

(13) Liu, X.; Schlexer, P.; Xiao, J.; Ji, Y.; Wang, L.; Sandberg, R. B.; Tang, M.; Brown, K. S.; Peng, H.; Ringe, S.; Hahn, C.; Jaramillo, T. F.; Nørskov, J. K.; Chan, K. PH Effects on the Electrochemical Reduction of CO(2) towards C2 Products on Stepped Copper. *Nat. Commun.* **2019**, *10* (1), 32.

(14) Resasco, J.; Chen, L. D.; Clark, E.; Tsai, C.; Hahn, C.; Jaramillo, T. F.; Chan, K.; Bell, A. T. Promoter Effects of Alkali Metal Cations on the Electrochemical Reduction of Carbon Dioxide. *J. Am. Chem. Soc.* **2017**, *139* (32), 11277−11287.

(15) Hori, Y.; Takahashi, I.; Koga, O.; Hoshi, N. Electrochemical Reduction of Carbon Dioxide at Various Series of Copper Single Crystal Electrodes. *J. Mol. Catal. A: Chem.* **2003**, *199* (1), 39−47.

(16) Jeon, H. S.; Kunze, S.; Scholten, F.; Roldan Cuenya, B. Prism-Shaped Cu Nanocatalysts for Electrochemical CO2 Reduction to Ethylene. *ACS Catal.* **2018**, *8* (1), 531−535.

(17) Hahn, C.; Hatsukade, T.; Kim, Y.-G.; Vailionis, A.; Baricuatro, J. H.; Higgins, D. C.; Nitopi, S. A.; Soriaga, M. P.; Jaramillo, T. F. Engineering Cu Surfaces for the Electrocatalytic Conversion of CO $_2$: Controlling Selectivity toward Oxygenates and Hydrocarbons. *Proc. Natl. Acad. Sci. U. S. A.* **2017**, *114* (23), 5918−5923.

(18) Zhang, B.; Zhang, J.; Hua, M.; Wan, Q.; Su, Z.; Tan, X.; Liu, L.; Zhang, F.; Chen, G.; Tan, D.; Cheng, X.; Han, B.; Zheng, L.; Mo, G. Highly Electrocatalytic Ethylene Production from CO2 on Nano-defective Cu Nanosheets. *J. Am. Chem. Soc.* **2020**, *142* (31), 13606−13613.

(19) Wang, Y.; Wang, Z.; Dinh, C.-T.; Li, J.; Ozden, A.; Golam Kibria, M.; Seifitokaldani, A.; Tan, C.-S.; Gabardo, C. M.; Luo, M.; Zhou, H.; Li, F.; Lum, Y.; McCallum, C.; Xu, Y.; Liu, M.; Proppe, A.; Johnston, A.; Todorovic, P.; Zhuang, T.-T.; Sinton, D.; Kelley, S. O.; Sargent, E. H. Catalyst Synthesis under CO2 Electroreduction Favours Faceting and Promotes Renewable Fuels Electrosynthesis. *Nat. Catal.* **2020**, *3* (2), 98−106.

(20) Singh, M. R.; Kwon, Y.; Lum, Y.; Ager, J. W.; Bell, A. T. Hydrolysis of Electrolyte Cations Enhances the Electrochemical Reduction of CO2 over Ag and Cu. *J. Am. Chem. Soc.* **2016**, *138* (39), 13006−13012.

(21) Lum, Y.; Ager, J. W. Sequential Catalysis Controls Selectivity in Electrochemical CO $_2$ Reduction on Cu. *Energy Environ. Sci.* **2018**, *11* (10), 2935−2944.

(22) Morales-Guio, C. G.; Cave, E. R.; Nitopi, S. A.; Feaster, J. T.; Wang, L.; Kuhl, K. P.; Jackson, A.; Johnson, N. C.; Abram, D. N.; Hatsukade, T.; Hahn, C.; Jaramillo, T. F. Improved CO 2 Reduction Activity towards C 2+ Alcohols on a Tandem Gold on Copper Electrocatalyst. *Nat. Catal.* **2018**, *1* (10), 764−771.

(23) Zhong, M.; Tran, K.; Min, Y.; Wang, C.; Wang, Z.; Dinh, C.-T.; De Luna, P.; Yu, Z.; Rasouli, A. S.; Brodersen, P.; Sun, S.; Voznyy, O.; Tan, C.-S.; Askerka, M.; Che, F.; Liu, M.; Seifitokaldani, A.; Pang, Y.; Lo, S.-C.; Ip, A.; Ulissi, Z.; Sargent, E. H. Accelerated Discovery of CO 2 Electrocatalysts Using Active Machine Learning. *Nature* **2020**, *581* (7807), 178−183.

(24) Wang, J.; Cheng, T.; Fenwick, A. Q.; Baroud, T. N.; Rosas-Hernández, A.; Ko, J. H.; Gan, Q.; Goddard III, W. A.; Grubbs, R. H. Selective CO $_2$ Electrochemical Reduction Enabled by a Tricomponent Copolymer Modifier on a Copper Surface. *J. Am. Chem. Soc.* **2021**, *143* (7), 2857−2865.

(25) Wei, X.; Yin, Z.; Lyu, K.; Li, Z.; Gong, J.; Wang, G.; Xiao, L.; Lu, J.; Zhuang, L. Highly Selective Reduction of CO2 to C2+ Hydrocarbons at Copper/Polyaniline Interfaces. *ACS Catal.* **2020**, *10* (7), 4103−4111.

(26) Chen, X.; Chen, J.; Alghoraibi, N. M.; Henckel, D. A.; Zhang, R.; Nwabara, U. O.; Madsen, K. E.; Kenis, P. J. A.; Zimmerman, S. C.; Gewirth, A. A. Electrochemical CO 2 -to-Ethylene Conversion on Polyamine-Incorporated Cu Electrodes. *Nat. Catal.* **2021**, *4* (1), 20−27.

(27) Buckley, A. K.; Lee, M.; Cheng, T.; Kazantsev, R. V.; Larson, D. M.; Goddard III, W. A.; Toste, F. D.; Toma, F. M. Electrocatalysis at Organic−Metal Interfaces: Identification of Structure−Reactivity Relationships for CO $_2$ Reduction at Modified Cu Surfaces. *J. Am. Chem. Soc.* **2019**, *141* (18), 7355−7364.

(28) Banerjee, S.; Han, X.; Thoi, V. S. Modulating the Electrode−Electrolyte Interface with Cationic Surfactants in Carbon Dioxide Reduction. *ACS Catal.* **2019**, *9* (6), 5631−5637.

(29) Han, Z.; Kortlever, R.; Chen, H.-Y.; Peters, J. C.; Agapie, T. CO2 Reduction Selective for C ≥ 2 Products on Polycrystalline Copper with N-Substituted Pyridinium Additives. *ACS Cent. Sci.* **2017**, *3* (8), 853−859.

https://doi.org/10.1021/acscentsci.1c00860
ACS Cent. Sci. XXXX, XXX, XXX−XXX

(30) Gao, D.; Arán-Ais, R. M.; Jeon, H. S.; Roldan Cuenya, B. Rational Catalyst and Electrolyte Design for CO2 Electroreduction towards Multicarbon Products. *Nat. Catal.* **2019**, *2* (3), 198−210.
(31) He, J.; Dettelbach, K. E.; Salvatore, D. A.; Li, T.; Berlinguette, C. P. High-Throughput Synthesis of Mixed-Metal Electrocatalysts for CO2 Reduction. *Angew. Chem., Int. Ed.* **2017**, *56* (22), 6068−6072.
(32) Nam, D.-H.; De Luna, P.; Rosas-Hernández, A.; Thevenon, A.; Li, F.; Agapie, T.; Peters, J. C.; Shekhah, O.; Eddaoudi, M.; Sargent, E. H. Molecular Enhancement of Heterogeneous CO 2 Reduction. *Nat. Mater.* **2020**, *19* (3), 266−276.
(33) Thevenon, A.; Rosas-Hernández, A.; Peters, J. C.; Agapie, T. In-Situ Nanostructuring and Stabilization of Polycrystalline Copper by an Organic Salt Additive Promotes Electrocatalytic CO_2 Reduction to Ethylene. *Angew. Chem., Int. Ed.* **2019**, *58* (47), 16952−16958.
(34) Li, F.; Thevenon, A.; Rosas-Hernández, A.; Wang, Z.; Li, Y.; Gabardo, C. M.; Ozden, A.; Dinh, C. T.; Li, J.; Wang, Y.; Edwards, J. P.; Xu, Y.; McCallum, C.; Tao, L.; Liang, Z.-Q.; Luo, M.; Wang, X.; Li, H.; O'Brien, C. P.; Tan, C.-S.; Nam, D.-H.; Quintero-Bermudez, R.; Zhuang, T.-T.; Li, Y. C.; Han, Z.; Britt, R. D.; Sinton, D.; Agapie, T.; Peters, J. C.; Sargent, E. H. Molecular Tuning of CO 2 -to-Ethylene Conversion. *Nature* **2020**, *577* (7791), 509−513.
(35) Thevenon, A.; Rosas-Hernández, A.; Fontani Herreros, A. M.; Agapie, T.; Peters, J. C. Dramatic HER Suppression on Ag Electrodes via Molecular Films for Highly Selective CO2 to CO Reduction. *ACS Catal.* **2021**, *11* (8), 4530−4537.
(36) Ren, D.; Fong, J.; Yeo, B. S. The Effects of Currents and Potentials on the Selectivities of Copper toward Carbon Dioxide Electroreduction. *Nat. Commun.* **2018**, *9* (1), 925.
(37) Hori, Y. Electrochemical CO_2 Reduction on Metal Electrodes. In *Modern Aspects of Electrochemistry*; Vayenas, C. G., White, R. E., Gamboa-Aldeco, M. E., Eds.; Springer: New York, 2008; Vol. *42*, pp 89−189.
(38) Kortlever, R.; Shen, J.; Schouten, K. J. P.; Calle-Vallejo, F.; Koper, M. T. M. Catalysts and Reaction Pathways for the Electrochemical Reduction of Carbon Dioxide. *J. Phys. Chem. Lett.* **2015**, *6* (20), 4073−4082.
(39) Hori, Y.; Murata, A.; Takahashi, R. Formation of Hydrocarbons in the Electrochemical Reduction of Carbon Dioxide at a Copper Electrode in Aqueous Solution. *J. Chem. Soc., Faraday Trans. 1* **1989**, *85* (8), 2309.
(40) Murata, A.; Hori, Y. Product Selectivity Affected by Cationic Species in Electrochemical Reduction of CO_2 and CO at a Cu Electrode. *Bull. Chem. Soc. Jpn.* **1991**, *64* (1), 123−127.
(41) Saberi Safaei, T.; Mepham, A.; Zheng, X.; Pang, Y.; Dinh, C.-T.; Liu, M.; Sinton, D.; Kelley, S. O.; Sargent, E. H. High-Density Nanosharp Microstructures Enable Efficient CO_2 Electroreduction. *Nano Lett.* **2016**, *16* (11), 7224−7228.
(42) Cheng, T.; Xiao, H.; Goddard, W. A. Full Atomistic Reaction Mechanism with Kinetics for CO Reduction on Cu(100) from Ab Initio Molecular Dynamics Free-Energy Calculations at 298 K. *Proc. Natl. Acad. Sci. U. S. A.* **2017**, *114* (8), 1795−1800.
(43) Garza, A. J.; Bell, A. T.; Head-Gordon, M. Mechanism of CO2 Reduction at Copper Surfaces: Pathways to C2 Products. *ACS Catal.* **2018**, *8* (2), 1490−1499.
(44) Schreier, M.; Yoon, Y.; Jackson, M. N.; Surendranath, Y. Competition between H and CO for Active Sites Governs Copper-Mediated Electrosynthesis of Hydrocarbon Fuels. *Angew. Chem., Int. Ed.* **2018**, *57* (32), 10221−10225.
(45) Xiao, H.; Cheng, T.; Goddard, W. A. Atomistic Mechanisms Underlying Selectivities in C_1 and C_2 Products from Electrochemical Reduction of CO on Cu(111). *J. Am. Chem. Soc.* **2017**, *139* (1), 130−136.
(46) Other potential ways to disrupt the scaling relationship observed here include nanostructuring,[16−18] higher overpotentials and current densities resulting in pH gradients,[12−15,20] and bimetallic system engineering.[21−23]

https://doi.org/10.1021/acscentsci.1c00860
ACS Cent. Sci. XXXX, XXX, XXX−XXX